Computer Physics Communications 315 (2025) 109733

Contents lists available at ScienceDirect

Computer Physics Communications

journal homepage: www.elsevier.com/locate/cpc

Computational Physics

Data-driven reduced modeling of streamer discharges in air

Jannis Teunissen [a,*], Alejandro Malagón-Romero [a,b]

[a] Centrum Wiskunde & Informatica (CWI), Science Park 123, Amsterdam, 1098 XG, the Netherlands
[b] Instituto de Astrofísica de Andalucía (IAA), CSIC, Glorieta de la Astronomía s/n, Granada, 18008, Spain

ARTICLE INFO

The review of this paper was arranged by Prof. Andrew Hazel

Dataset link: https://github.com/jannisteunissen/cocydimo, https://doi.org/10.5281/zenodo.15296406

Keywords:
Electric discharge
Streamer discharge
Reduced model
Data-driven model

ABSTRACT

We present a computational framework for simulating filamentary electric discharges, in which channels are represented as conducting cylindrical segments. The framework requires a model that predicts the position, radius, and line conductivity of channels at a next time step. Using this information, the electric conductivity on a numerical mesh is updated, and the new electric potential is computed by solving a variable-coefficient Poisson equation. A parallel field solver with support for adaptive mesh refinement is used, and the framework provides a Python interface for easy experimentation. We demonstrate how the framework can be used to simulate positive streamer discharges in air. First, a dataset of 1000 axisymmetric positive streamer simulations is generated, in which the applied voltage and the electrode geometry are varied. Fit expressions for the streamer radius, velocity, and line conductivity are derived from this dataset, taking as input the size of the high-field region ahead of the streamers. We then construct a reduced model for positive streamers in air, which includes a stochastic branching model. The reduced model compares well with the axisymmetric simulations from the dataset, while allowing spatial and temporal step sizes that are several orders of magnitude larger. 3D simulations with the reduced model resemble experimentally observed discharge morphologies. The model runs efficiently, with 3D simulations with 20+ streamers taking 4–8 minutes on a desktop computer.

1. Introduction

Streamer discharges are the precursors of lightning leaders and sparks, they occur above thunderstorms as sprites, and they are used in diverse technological applications [1]. Streamers develop non-linearly at velocities of 10^5 to 10^7 m/s, forming conducting channels with strong electric field enhancement at their tips. The enhanced field causes the conductive channels to grow due to rapid electron impact ionization. Numerical simulations have become a valuable tool to understand and predict streamer discharges. Simulations are usually performed with a fluid model, see e.g. [2–8], although particle simulations are sometimes also used, see e.g. [9,10]. The cost of such 'microscopic' simulations is typically quite high, because a high temporal and spatial resolution is required to resolve the electron dynamics.

The two main processes that drive a streamer discharge are electron impact ionization and electron drift. Accurately describing the spatial growth of the electron density in a fluid or particle model requires a grid spacing

$$\Delta x \lesssim 1/|\bar{\alpha}|, \tag{1}$$

where $\bar{\alpha} = \alpha - \eta$ is the Townsend ionization coefficient minus the attachment coefficient. Accurately resolving the temporal growth of the electron density generally requires a time step

$$\Delta t \lesssim 1/|\bar{\alpha}\,\mathbf{v}_d|, \tag{2}$$

where $\mathbf{v}_d = -\mu_e \mathbf{E}$ is the electron drift velocity, μ_e the electron mobility and $\mathbf{E}$ the electric field. The right-hand side is the inverse of the effective electron impact ionization rate, but it can also be thought of as a resulting from a CFL-like condition $\Delta t \lesssim \Delta x/v_d$, with Δx given by equation (1). The above time step restriction also applies to models that use implicit time integration if an accurate solution is required, as discussed in [11].

Fig. 1 shows data for $\bar{\alpha}$ and μ_e for air at 1 bar and 300 K. A typical streamer in air has a maximum electric field $E_{\max}$ at its tip between 100 kV/cm and 250 kV/cm. In this range, $\bar{\alpha}$ is approximately proportional to the electric field strength E, and so is the drift velocity, since μ_e is approximately constant. This means that $\Delta x \propto (E_{\max})^{-1}$ and $\Delta t \propto (E_{\max})^{-2}$, so that the cost of a uniform-grid 3D simulation will approximately scale as $(\Delta x)^{-3}\,(\Delta t)^{-1} \sim (E_{\max})^5$. Fig. 1 shows that Δx will range from about 10 μm to 2.5 μm for fields between 100 kV/cm and

* Corresponding author.
E-mail address: jannis.teunissen@cwi.nl (J. Teunissen).

https://doi.org/10.1016/j.cpc.2025.109733
Received 10 January 2025; Received in revised form 19 June 2025; Accepted 27 June 2025
Available online 4 July 2025

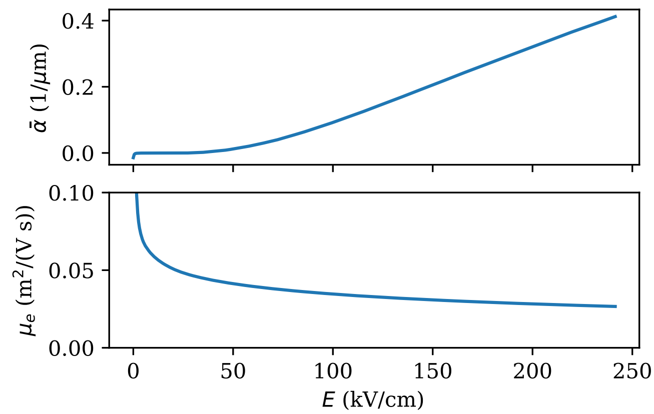

Fig. 1. The effective ionization coefficient $\bar{\alpha}$ and electron mobility μ_e for electrons in air (80% N_2, 20% O_2) at 1 bar and 300 K, computed from Phelps's cross sections [12,13].

250 kV/cm, whereas streamer discharges in air can measure centimeters or more. Most 3D simulations are therefore performed with adaptive mesh refinement (AMR), see e.g. [14–17,6]. However, even then there are many cases of interest that are currently too expensive to simulate, for example because the discharge contains too many streamer channels, or because the evolution on large spatial or temporal scales is of interest.

Several authors have developed reduced models in which the smallest spatial and temporal scales for electrons do not have to be resolved. In the dielectric breakdown model (DBM) [18], the domain is separated into conducting and non-conducting cells. The conducting region expands stochastically, one cell at a time, with the probability depending on the local electric field strength. In [19], this type of model was modified for the simulation of sprite discharges, and in [20], the model was adapted for simulating discharge treeing in solid dielectrics. A somewhat related model was developed in [21], in which streamers were modeled as segments of perfectly conducting cylinders, and a finite-element solver was used to compute the electric field configuration of the discharge. To improve some shortcomings of the above models, a 'tree model' was presented in [22] and further refined in [23]. In these tree models, the channels are approximated by a series of point or ring charges, with the radius, conductivity and charge density evolving along the channel. The electric field and the electric current are computed self-consistently by including the pair-wise interactions between all point or ring charges. Although more physics is included than in the DBM models, these tree models still require some ad-hoc parameters, such as a prescription for the streamer radius.

In this paper, we make several contributions to the development of reduced models for electric discharges. In section 2 we present a framework for simulating the growth of imperfectly conducting cylinders in a self-consistent electric field. As input, a growth model for the cylinders and their conductivity is required. The conductivity of the cylinders is mapped to a numerical mesh, and by solving a modified Poisson equation on this mesh the electric potential at the next time step can be found. The field solver includes adaptive mesh refinement and support for electrodes using the `afivo` [24] library, and the resulting code is converted to a Python module. The growth model for the cylinders can be fully written in Python, allowing for easy experimentation with different types of data-driven or physics-based models.

Next, we describe a dataset of 1000 axisymmetric positive streamer simulations in section 3. The simulations are performed in air at 1 bar and 300 K, while the applied voltage and the electrode geometry are varied. From the dataset, we fit a simple model for the streamer radius, velocity and conductivity, taking as input a length scale of the high-field region around the streamer head. Based on these expressions, we construct a reduced model for streamer growth in section 4, using the framework described in section 2. With this model, the grid spacing and time step can be much larger than the restrictions given by equations (1) and (2). Finally, we compare the model's prediction to the original fluid simulation in the dataset, and we show examples of 3D simulations in section 5.

2. Framework for growing conducting cylinders in an electric field

Streamers and lightning leaders are examples of filamentary electric discharges, typically consisting of many conductive channels that rapidly grow and sometimes branch. Below, we will describe a basic framework to simulate such phenomena. One assumption underlying our approach is that channels have a highly similar shape with a rounded head, as has been observed in many simulations and experiments. This allows us to describe each channel as a collection of conducting cylindrical segments with a semi-spherical cap at the end. It is assumed that channels propagate parallel to the electric field ahead of them, and the radial electron density profile inside each channel is assumed to be fixed.

Another important assumption is that much of the complex dynamics of a discharge results from electrostatic interactions. The framework was designed to capture these electrostatic interactions rather well. The streamer conductivity is therefore represented on a numerical mesh that is fine enough to resolve the streamer radii and the electric field profiles around streamer heads. This mesh is a structured grid with quadtree/octree type grid refinement, and its spacing can be hundreds of µm for streamer discharges in atmospheric air, as we will show in section 5.2.

It is assumed that some model is available to predict the position $\mathbf{r}$, radius R and line conductivity σ_line of each channel at the next time step. This information can be used to update the conductivity in the domain, by adding cylindrical segments representing the extension of each channel, as described in section 2.1. Afterwards, the electric potential at the new time step can be computed on the numerical mesh as described in section 2.2. As will be discussed in section 5.2, time steps in the reduced model can be two to three orders of magnitude larger than in conventional streamer simulations.

2.1. Conducting cylinders

The conducting channels will be represented by cylindrical segments with a semi-spherical cap at the end. It is assumed that some model is available to predict the following properties:

- The next radius $R(t + \Delta t)$.
- The next position $\mathbf{r}(t + \Delta t)$, located at the center of the semi-spherical cap, as illustrated in Fig. 2.
- The next line conductivity $\sigma_\mathrm{line}(t + \Delta t)$, where the line conductivity is defined as the integral over the conductivity over the channel's cross-section.

Furthermore, we assume there is a function $f_r(d_r/R)$ that describes the radial conductivity profile, where d_r is the distance from the cylinder's axis. With the above information, a cylindrical segment can be added between $\mathbf{r}(t)$ and $\mathbf{r}(t + \Delta t)$, see Fig. 2. To update the conductivity on the mesh, the following conditions are checked for every grid cell:

- $d < R(t + \Delta t)$, where d is the distance from the cell center to the nearest point of the line segment between $\mathbf{r}(t)$ and $\mathbf{r}(t + \Delta t)$. This condition is fulfilled inside a cylindrical segment of radius $R(t + \Delta t)$ with semi-spherical caps.
- $d_0 > R(t)$, where d_0 is the distance to the previous position $\mathbf{r}(t)$. This excludes the cap of the previous segment. Furthermore, the cell should be closer to $\mathbf{r}(t + \Delta t)$ than it is to $\mathbf{r}(t) - [\mathbf{r}(t + \Delta t) - \mathbf{r}(t)]$, which prevents adding conductivity behind the previous cap when the radius increases.

Fig. 2. Illustration of how cylindrical segments with a semi-spherical cap can be added together to extend a channel from $\mathbf{r}_1$ to $\mathbf{r}_2$ (left) and afterwards from $\mathbf{r}_2$ to $\mathbf{r}_3$ (right). We assume a constant radius R along an individual segment. Note that the respective $\mathbf{r}$ coordinates are defined at the 'center' of the segment's caps. The figure is not to scale: in actual simulations, the length of a newly added segment is comparable to the streamer radius or smaller, see section 4.3.

When these criteria a met, the change in conductivity in a grid cell is given by

$$\sigma_{\text{new}} = \sigma_{\text{old}} + \sigma^*_{\text{line}} \frac{f_r(d_r/R)}{\pi R^2}, \tag{3}$$

where σ^*_{line} is obtained by linearly interpolating between $\sigma_{\text{line}}(t)$ at $\mathbf{r}(t)$ and $\sigma_{\text{line}}(t+\Delta t)$ at $\mathbf{r}(t+\Delta t)$. Note that the radial profile $f_r(x)$ should be normalized so that

$$\int_0^\infty 2\pi r \frac{f_r(r/R)}{\pi R^2} \, dr = 1. \tag{4}$$

As discussed in Appendix A, we here use a truncated parabola [22,25] for the radial profile

$$f_r(x) = \max\left[0, 2\,(1-x^2)\right]. \tag{5}$$

We remark that there are several definitions of the streamer radius R, e.g., optical and electrodynamic. In equations (3)–(5) R should be the effective radius of the conductivity profile. Later in this paper we will refer to this radius as R_σ.

2.2. Evolving conductivity and potential

The procedure described in section 2.1 can be used to obtain the conductivity at the next time step $\sigma(\mathbf{r}, t+\Delta t)$. Below, we discuss how the new electric potential $\phi(t+\Delta t)$ can be computed using $\sigma(t+\Delta t)$, where have dropped the dependence on $\mathbf{r}$ for brevity. Recall that the electric potential ϕ is the solution of

$$\nabla^2 \phi = -\rho/\varepsilon_0, \tag{6}$$

where ρ is the charge density. From the conservation of charge, it follows that

$$\partial_t \rho = -\nabla \cdot \mathbf{J} \approx -\nabla \cdot (\sigma \mathbf{E}) = \nabla \cdot (\sigma \nabla \phi), \tag{7}$$

where we approximated the current density as $\mathbf{J} \approx \sigma \mathbf{E}$, ignoring the effects of diffusion, and used $\mathbf{E} = -\nabla\phi$. Integrating equation (7) over time gives

$$\rho(t+\Delta t) = \rho(t) + \int_t^{t+\Delta t} \nabla \cdot [\sigma(t')\nabla\phi(t')]\,\mathrm{d}t', \tag{8}$$

so that

$$\nabla^2 \phi(t+\Delta t) = -\frac{\rho(t)}{\varepsilon_0} - \frac{1}{\varepsilon_0} \int_t^{t+\Delta t} \nabla \cdot [\sigma(t')\nabla\phi(t')]\,\mathrm{d}t'. \tag{9}$$

We use a first-order accurate backward-Euler scheme to solve this equation, by approximating $\phi(t') = \phi(t+\Delta t)$ and $\sigma(t') = \sigma(t+\Delta t)$ inside the integral, which results in

$$\nabla \cdot [\varepsilon_\sigma \nabla \phi(t+\Delta t)] = -\rho(t)/\varepsilon_0, \tag{10}$$

$$\varepsilon_\sigma = 1 + \Delta t\, \sigma(t+\Delta t)/\varepsilon_0. \tag{11}$$

This is the same variable-coefficient elliptic PDE as is solved when using a so-called semi-implicit scheme in discharge simulations [26,27].

We solve equation (10) using the geometric multigrid methods implemented in the `afivo` library [24,28]. The `afivo` library supports OpenMP parallelization, grid refinement (of the quadtree/octree type), and it is possible to include curved electrodes using a level-set function [28]. Equation (10) is solved using FMG (full multigrid) cycles, until the residual is smaller than $10^{-5} \max(|\rho(t)|/\varepsilon_0)$. Due to the variable coefficient, this typically takes about 4-6 FMG cycles.

After $\phi(t+\Delta t)$ has been obtained, we use equation (6) to compute $\rho(t+\Delta t)$. The degree to which charge is conserved, except for currents through the domain boundaries, depends on the accuracy with which equation (10) is solved. If the Poisson equation is solved up to machine precision, charge will be conserved approximately up to machine precision.

2.3. Implementation as a Python module

To make it easier to experiment with different types of models, we have separated the implementation into a Fortran and a Python part. The computationally expensive parts are all implemented in Fortran, for example the solution of equation (10), and the updating of the electric conductivity on the mesh. With `F2PY` (Fortran to Python interface generator), this Fortran code was converted to a Python module. The most important methods available through this module are:

- A method to update the conductivity in the domain, given the new and previous channel positions $\mathbf{r}_i$, radii R_i and line conductivities $\sigma_{\text{line},i}$.
- A method to solve the Poisson equation given by (10).
- Functions to initialize the computational domain (size, minimum grid spacing, refinement criteria), the applied voltage, and the electrode geometry.
- A method to store a field-dependent effective ionization rate, which is used to update the conductivity inside channels according to equation (23).
- Methods to get the electric field vector at a location, to get the location of the maximum field, and to interpolate a variable (electric potential, electric field strength, conductivity) along a line on the mesh.
- A method to update the adaptive mesh refinement.
- A method to write the mesh variables to a Silo file, that can be visualized using e.g. Visit [29].

The framework can be used in both 2D and 3D. To avoid duplicating code for 2D and 3D, a header file with several macros is included in the Fortran source code (provided by the `afivo` library [24]), so that the number of dimensions can be specified at compile time. By default, no mesh refinement is performed in 2D, since 2D simulations are computationally not expensive.

3. Simulation dataset

The framework described in section 2 requires a method that predicts the next radius, velocity and line conductivity of each channel. For this purpose, we have constructed a dataset of axisymmetric simulations of positive streamers in air by varying the applied voltage and electrode geometry, from which we derive simple fit formulas for streamer parameters.

3.1. Fluid model and simulation conditions

The simulations are performed with the classical drift-diffusion-reaction fluid model using the open-source `afivo-streamer` code [24,17]. In this model, the electron density n_e evolves in time as

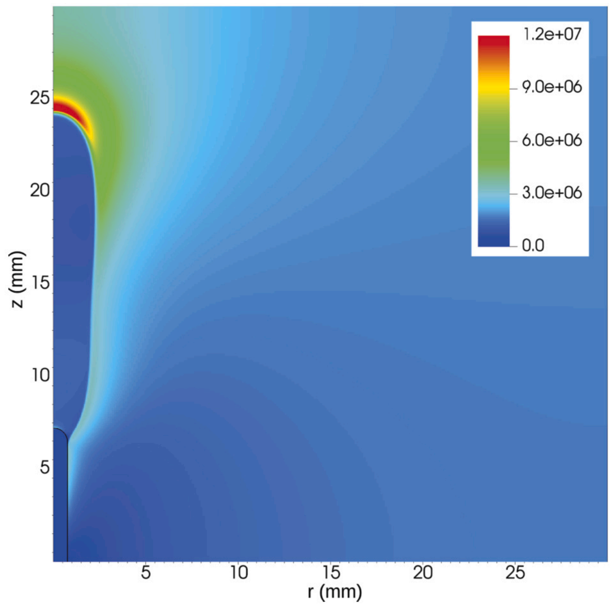

Fig. 3. Example of the electric field distribution in one of the axisymmetric streamer simulations. The boundary of the needle electrode at the bottom left is marked with a line.

$$\partial_t n_e = \nabla \cdot (\mu_e \mathbf{E} n_e + D_e \nabla n_e) + S_e + S_{\mathrm{ph}}, \tag{12}$$

where μ_e is the electron mobility coefficient, D_e is the diffusion coefficient, $\mathbf{E}$ is the electric field, S_e is a source (and sink) term of free electrons due to reactions, and S_{ph} is the photo-ionization source term. The motion of ions is not taken into account, so their densities only change in time due to source terms. The simulations are performed in artificial air, consisting of 80% N_2 and 20% O_2 at 1 bar and 300 K. We use the same reactions and transport data as e.g. [30], computed using BOLSIG- [31] using Phelps' cross-section data for N_2 and O_2 [12,13]. The photoionization source term S_{ph} is computed using the Zheleznyak model of [32] and the Helmholtz approximation, see e.g. [11].

The axisymmetric computational domain is illustrated in Fig. 3. It measures 30 mm in the r and z direction, and it has a plate-plate geometry. A rod-shape needle electrode placed at the bottom plate provides initial field enhancement so that a positive streamer can start. This needle is shaped as a cylinder with a semi-spherical cap, and its length and radius are varied as described in section 3.2. In order for discharges to start, a small background ionization density $n_0 = 10^{11}\,\mathrm{m}^{-3}$ of electrons and N_2^+ ions is included.

The electric field $\mathbf{E}$ is calculated as $\mathbf{E} = -\nabla\phi$, where ϕ is the electrostatic potential, obtained by solving the Poisson equation with a multigrid method [24,28]. The electric potential is fixed on the bottom and top of the domain, with the needle electrode at the same voltage as the bottom plate. Homogeneous Neumann boundary conditions are used on the radial boundary.

At the needle electrode, electrons are absorbed but not emitted. On the domain boundaries, homogeneous Neumann boundary conditions are used for the electron density, but simulations stop before this becomes relevant. All simulations are performed with adaptive mesh refinement (AMR), using the refinement criterion $\alpha(E)\Delta x \leq 1$, where $\alpha(E)$ is the Townsend ionization coefficient. The mesh refinement provided by the `afivo` library [24] is of the quadtree/octree type, with a refinement ratio of two between levels. Time integration is performed explicitly with a second-order accurate Runge-Kutta scheme, so the time step Δt is limited by a CFL (Courant–Friedrichs–Lewy) condition, see [17] for details. The finest grid spacing required for the dataset described below was $\Delta x = 1.8$ µm, although for most cases $\Delta x = 3.7$ µm was sufficient. For $\Delta x = 3.7$ µm, time steps were typically on the order of $\Delta t \sim 2\,\mathrm{ps}$.

3.2. Description of dataset

We generate a dataset of 1000 axisymmetric streamer simulations in which the following parameters are varied:

- The radius R_{rod} of the rod electrode is drawn from a uniform distribution between $R_{\mathrm{min}} = 0.5\,\mathrm{mm}$ and $R_{\mathrm{max}} = 1.5\,\mathrm{mm}$
- The length of the rod electrode is scaled linearly with its radius as

$$L_{\mathrm{rod}} = L_{\mathrm{min}} + (L_{\mathrm{max}} - L_{\mathrm{min}}) \frac{R_{\mathrm{rod}} - R_{\mathrm{min}}}{R_{\mathrm{max}} - R_{\mathrm{min}}},$$

  using $L_{\mathrm{max}} = 12\,\mathrm{mm}$ and $L_{\mathrm{min}} = 4.5\,\mathrm{mm}$.
- The applied voltage V_0 is drawn from a uniform distribution between $V_{\mathrm{min}} = 36\,\mathrm{kV}$ and $V_{\mathrm{max}} = 60\,\mathrm{kV}$.

With these applied voltages, the background electric fields E_{bg} between the two parallel plates range from 12 kV/cm to 20 kV/cm. Each simulation is stopped when the distance to the opposite electrode is 5 mm. Streamer velocities vary significantly with the above parameters. To obtain about 30 output files per simulation, we empirically scale the time step for writing output $\Delta t_{\mathrm{output}}$ with E_{avg}^{-2}, where E_{avg} is the average electric field between the tip of the rod electrode and the opposite plate electrode. The dataset consists of approximately 3×10^4 output files, which contain the species densities, electric field and electric potential in the full simulation domain. To allow for easier processing, these files (with AMR) are converted to a uniform resolution of 256^2. We extract several quantities from the simulation data:

- The maximum electric field at the streamer head E_{max}.
- The z-coordinate where E_{max} occurs, called z_{head}.
- The streamer velocity v, defined as

$$v = \left[z_{\mathrm{head}}(t) - z_{\mathrm{head}}(t - \Delta t)\right] / \Delta t,$$

  where Δt is the time step between writing output.
- The streamer electrodynamic radius R_E, defined as the radial coordinate at which the radial electric field E_r has a maximum. Note that R_E is determined over the entire streamer head, not restricted to $z = z_{\mathrm{head}}$.
- The effective radius R_σ of the streamer's radial conductivity profile. As discussed in Appendix A, we approximate this radius as

$$R_\sigma = 1.2\, R_E. \tag{13}$$

- The line conductivity due to electrons

$$\sigma(z) = 2\pi e \int_0^\infty r\, \mu_e(r, z)\, n_e(r, z)\, dr, \tag{14}$$

  where e is the elementary charge. We define line conductivity at the head as

$$\sigma_{\mathrm{h}} = \sigma(z_{\mathrm{head}} - R_E), \tag{15}$$

  for a streamer propagating in the $+z$ direction, since we observed that the maximum line conductivity typically occurred about one radius behind z_{head}.
- The size L_E of the high-field region ahead of a streamer, defined as the distance between z_{head} and the z-coordinate where the electric field drops below a threshold of $E_{\mathrm{threshold}} = 50\,\mathrm{kV/cm}$.

Fig. 4 shows the distributions and relations between the above-listed parameters in the dataset. Note that σ_{h} and L_E were determined from the 256^2 uniform data, whereas the other parameters were extracted from the original simulation files. Because the measurements of R_E are somewhat noisy, we applied a Savitzky-Golay filter of width 5 and order 2 to the data from each run. Furthermore, for each run, the first two outputs were excluded from the dataset.

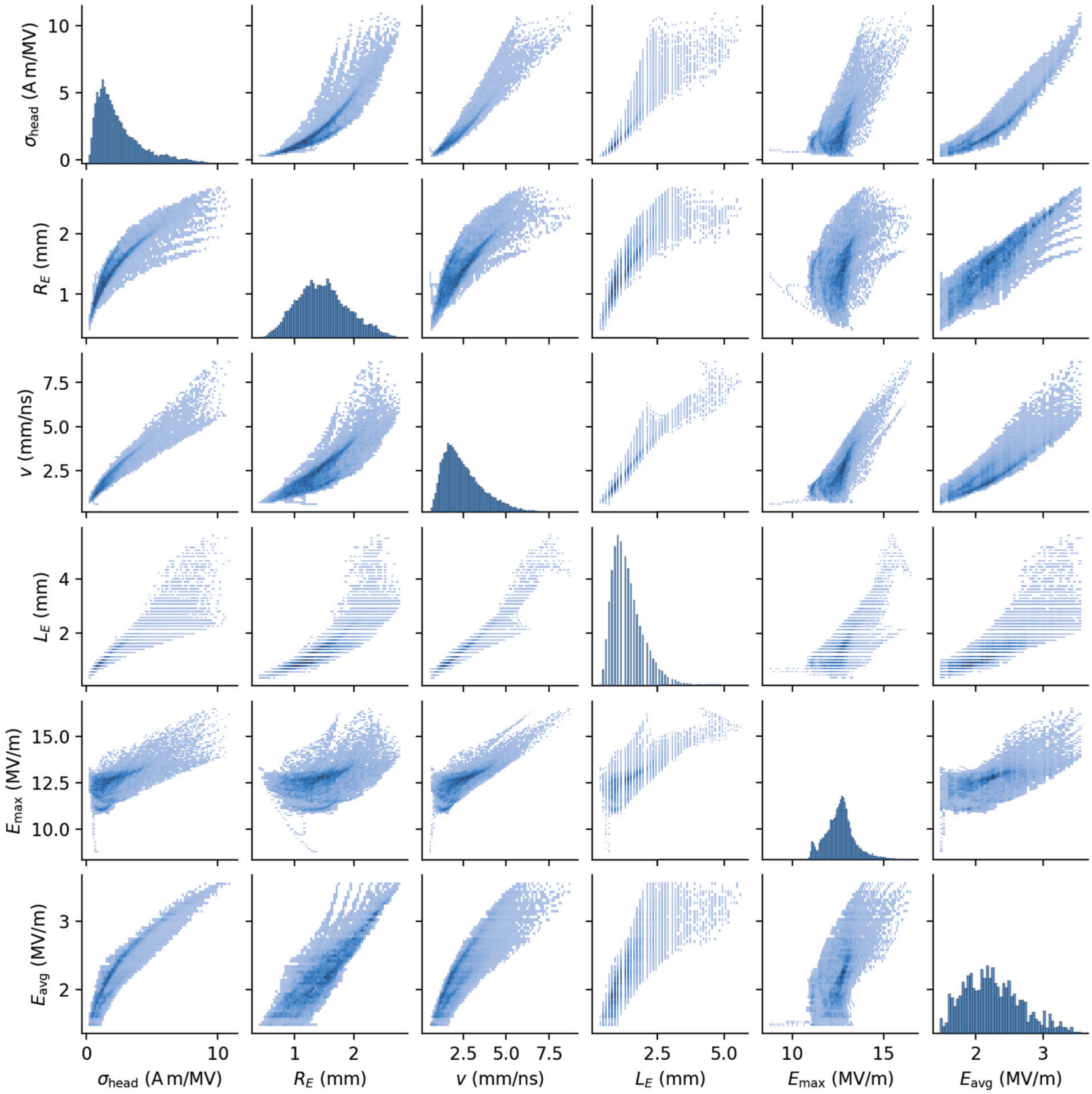

Fig. 4. Pairwise relationships between parameters extracted from 1000 axisymmetric positive streamer simulations in air at 1 bar and 300 K. On the diagonal the distributions of the parameters are shown.

L_E is a relevant length scale that can also be determined on coarse grids, as discussed in section 4.2. The threshold used to determine L_E is somewhat arbitrary, and we have experimented with several values ranging between 45 kV/cm and 60 kV/cm. Higher thresholds improved the ability to predict streamer properties from L_E (see section 3.3), but since L_E was then smaller, they also resulted in more noise when L_E was determined on a numerical grid.

3.3. A simple model for v, R and σ_h

From the dataset, we now construct a simple model to predict the electrodynamic radius R_E, the velocity magnitude v and the line conductivity at the streamer head σ_h. There are many ways to fit the curves shown in Fig. 4, but we here opt for the following approximations:

$$\sigma_h = \begin{cases} 1 \times 10^{-8} + 1.40\, L_E^2 & L_E < 10^{-3} \\ -1.41 \times 10^{-6} + 2.80 \times 10^{-3}\, L_E & L_E \geq 10^{-3} \end{cases} \tag{16}$$

$$R_E = \begin{cases} 2.90 \times 10^{-5} + 1.30\, L_E & L_E < 10^{-3} \\ 6.31 \times 10^{-4} + 0.627\, L_E & L_E \geq 10^{-3} \end{cases} \tag{17}$$

$$v = 1.78 \times 10^9\, L_E, \tag{18}$$

where the quantities are all made dimensionless using the following units: m for R_E and L_E, A m/V for σ_h, V/m for E_{avg} and m/s for v. Note that the expression for σ_h consists of a quadratic function for $L_E < 1$ mm, while for $L_E \geq 1$ mm the tangent line at $L_E = 1$ mm is used. For R_E a broken line is used, with the break also at $L_E = 1$ mm, and for v the fit is a single line. The reason for using broken curves in these fits is that we wanted to approximate both the behavior at small L_E and at large L_E reasonably well, while ensuring non-negativity of σ_h, R_E and v for $L_E \geq 0$. Furthermore, note that all expressions have a linear dependence on L_E for $L_E > 1$ mm.

In Fig. 5, equations (16)–(18) are compared against the dataset. The R^2 scores (coefficients of determination) are also given in the figure, with 1.0 being the highest possible value if there is no prediction error. Note that for large values of L_E, some predictions of R_E lie a bit further

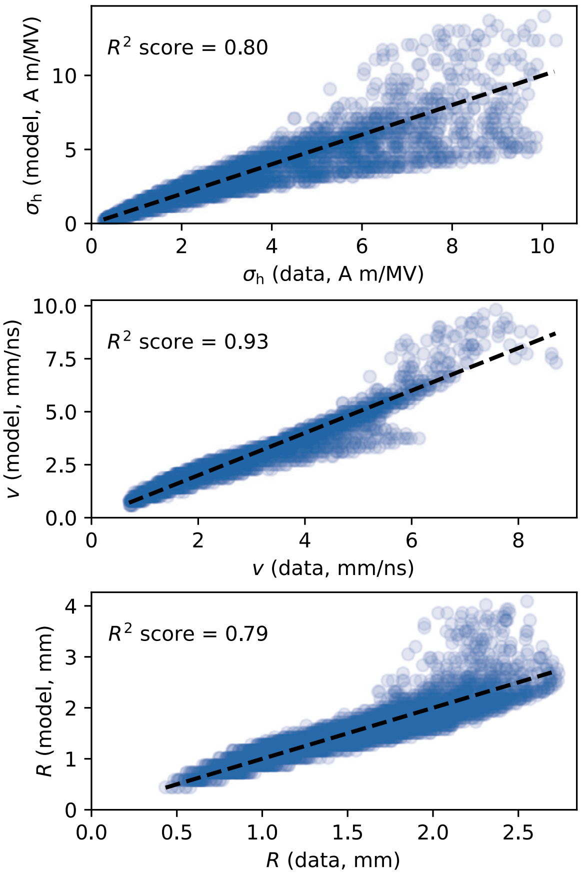

Fig. 5. A comparison of the simple model given by equations (16)–(18) against the simulation dataset. The model predictions are shown on the vertical axes, and the data on the horizontal axes. The dashed lines indicate were predictions and data are equal.

above the data. These points correspond to the moment the streamer is close to the opposite electrode, which causes L_E to increase faster than the radius.

To fit the above formulas, the data was split in a training set (70% of the runs) and a test set (30% of the runs). However, due to the limited number of parameters in the model, there was essentially no overfitting and thus almost no difference when we compared against the training or the test set.

3.4. Comments on dataset

The dataset described here has several limitations, even when only considering positive streamers in air. Due to the use of an axisymmetric model, the dataset does not contain streamer branching or streamer-interaction phenomena. Furthermore, the dataset contains no simulations in low background fields, in which streamers obtain a small radius and possibly stagnate [1], since such simulations can be somewhat challenging to perform [33–35]. Another limitation is that only a single type of electrode geometry was considered, namely two plates with a needle on one side and a fixed gap size.

With enough computational resources, one could construct a more general dataset based on 3D streamer simulations, including streamer branching, different electrode geometries, and different gap sizes. Since negative and positive streamers often form simultaneously, for example in a needle-to-needle geometry, it would make sense to include negative streamers in the dataset as well. The main challenges in constructing such a dataset are that the simulations are computationally expensive, that a significant amount of data needs to be stored, and that it is harder to extract features from such 3D data.

4. Reduced model for streamer discharges

We now describe a new reduced model for streamer discharges, which we have named `cocydimo` for "Conducting Cylinder Discharge Model". The model makes use of the framework described in section 2 and the dataset described in section 3.3. A schematic overview of the model is shown in Algorithm 1, and its main parameters are summarized in Table 1.

In a streamer discharge, the spatial conductivity profile $\sigma(\mathbf{r})$ rapidly changes at streamer heads due to electron impact ionization, and it changes more slowly inside the channels due to e.g. electron attachment. Below, we explain how we predict the conductivity at the next time step $\sigma(\mathbf{r}, t + \Delta t)$ from the previous conductivity $\sigma(\mathbf{r}, t)$, electric potential $\phi(\mathbf{r}, t)$ and the following streamer parameters:

- The radius R_σ of the streamer's radial conductivity profile.
- The position $\mathbf{r}$ at the 'center' of the streamer head, so that its conductivity is nonzero within a distance R_σ from $\mathbf{r}$.
- The propagation direction $\hat{\mathbf{v}}$, where the hat denotes a unit vector.

Once $\sigma(\mathbf{r}, t + \Delta t)$ is known, $\phi(\mathbf{r}, t + \Delta t)$ can be computed, as described in section 2.2.

Algorithm 1 Pseudocode for reduced discharge model.

```
Input: Specify computational domain, electrode geometry, applied voltage,
       time step, (finest) grid spacing
Initialize: Set streamer start location(s), t = 0

while t < t_end do
    for each channel do
        if 3D then                                              ▷ Sec. 4.5
            Sample τ_branch
            if τ_branch < Δt then
                Add new channel
                Sample branching angles
                Rotate channel directions

        Determine electric field direction Ê                    ▷ Sec. 4.1
        Measure L_E and apply smoothing                         ▷ Sec. 4.2
        Get new σ_h, R_σ and v from model                       ▷ Sec. 3.3
        Determine new location r                                ▷ Sec. 4.3

    Update mesh refinement (in 3D)                              ▷ Sec. 5.3
    Map conductivity of new segments to mesh                    ▷ Sec. 2.1
    Update conductivity in channels                             ▷ Sec. 4.4
    Compute new electric potential and field                    ▷ Sec. 2.2
    t = t + Δt
```

4.1. Determining the streamer propagation direction

In 3D, we assume that streamers propagate in the direction of the electric field ahead of them. This field is sampled at a location slightly in front of a streamer, given by

$$\mathbf{r}_E = \mathbf{r}(t) + (1 + c_{\text{ahead}})\, R_\sigma\, \hat{\mathbf{v}}(t), \tag{19}$$

where we use $c_{\text{ahead}} = 0.5$. There is a balance here: on the one hand, we want the field direction close to the streamer head, but if we get too close to the conductive region, this field direction will be rather noisy on a coarse mesh. However, the choice of $c_{\text{ahead}} = 0.5$ is somewhat arbitrary, and this value could be refined by carefully comparing streamer paths against conventional 3D simulations. After $\mathbf{r}_E$ has been determined, the new propagation direction is given by

$$\hat{\mathbf{v}}(t + \Delta t) = \hat{\mathbf{E}}(\mathbf{r}_E), \tag{20}$$

as illustrated in Fig. 6. In 2D axisymmetric simulations, streamers are simply assumed to propagate in the z direction.

Table 1
Summary of key variables and parameters in the reduced model.

Variable / parameter	Description	Value / given by
L_E	Size of the high-field region ahead of streamer	Eq. (21)
$E_{\text{threshold}}$	Threshold electric field for L_E determination	50 kV/cm
β	Smoothing coefficient for L_E in eq. (21)	0.5
c_1	Coefficient correcting for grid spacing bias in L_E in eq. (26)	0.75
$R_\sigma(t)$	Radius of streamer's conductivity profile	Eqs. (13), (17)
$\sigma_h(t)$	Line conductivity at streamer head	Eq. (16)
$\mathbf{r}(t)$	Position at 'center' of streamer head	Eq. (22)
$\mathbf{v}(t)$	Streamer velocity	Eqs. (18), (20)
c_{ahead}	Coefficient for sampling field direction in eqs. (19), (20)	0.5
$S(E)$	Effective ionization rate for updating channel conductivity in eq. (24)	Input data
c_b	Parameter for branching time in eq. (25)	10 – 20
L_b	Parameter for branching dependence on radius in eq. (25)	0.2 mm – 0.8 mm
Δt	Time step of the model, see section 5.2	up to 1 ns
Δx	Grid spacing for channels, see section 5.2	up to hundreds of µm

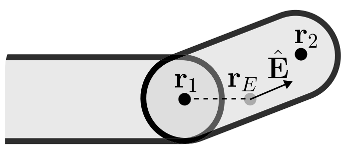

Fig. 6. Schematic illustration of the approach used to determine the propagation direction of a streamer. The electric field unit vector $\hat{\mathbf{E}}$ is sampled at $\mathbf{r}_E$ ahead of the channel. The new conducting segment then points towards $\hat{\mathbf{E}}$.

4.2. Determining L_E

To determine L_E, we sample the electric field strength along a line from $\mathbf{r}(t)$ extending towards the new propagation direction $\hat{\mathbf{v}}(t+\Delta t)$. Along this line, L_E is determined as the distance between the location of the maximum field to the location where $E \le E_{\text{threshold}}$. Such measurements of L_E are noisy, with fluctuations on the order of the grid spacing Δx, which can be quite large in the reduced model. To reduce these fluctuations, we use exponential smoothing for all but the first measurement:

$$L_{E,\text{new}} = \beta\, L^*_{E,\text{new}} + (1-\beta)\, L_{E,\text{old}}, \tag{21}$$

where $L^*_{E,\text{new}}$ is the new measurement and where we use a smoothing factor β. The value of β can be specified when running the model; unless stated otherwise we use $\beta = 0.5$. In section 5.2 we will discuss the dependence of L_E on the grid spacing Δx and how to correct for that.

Positive streamers can stagnate [33–35] when the background field they propagate in becomes too low. This phenomenon is common in 3D simulations in which some branches are overtaken by others. We assume streamers have stagnated when L_E drops below a threshold of $L_{E,\text{min}}$, and then halt their growth. For the simulations presented here we use $L_{E,\text{min}} = 0.1\,\text{mm}$, which corresponds to a minimal radius $R_{E,\text{min}} = 0.16\,\text{mm}$. Smaller radii have been observed in experiments and simulations [36,35], but only for rather slow 'minimal' streamers that are not represented in our dataset.

4.3. Updating the streamer position

Once L_E is known, equations (16)–(18) are used to obtain new values for σ_h, $R_\sigma = 1.2\,R_E$ and v. We limit the change ΔR_σ during a time step Δt to be at most $v\,\Delta t$, which avoids an instantaneous expansion of the radius during streamer inception. The new streamer position is computed as

$$\mathbf{r}(t+\Delta t) = \mathbf{r}(t) + \Delta t\, \mathbf{v}(t+\Delta t) - \Delta R_\sigma\, \hat{\mathbf{v}}(t+\Delta t), \tag{22}$$

where $\mathbf{v}(t+\Delta t) = v(t+\Delta t)\,\hat{\mathbf{v}}(t+\Delta t)$. The change in radius ΔR_σ is subtracted because $\mathbf{r}(t)$ is the position at the center of the streamer head, while we want the conductive region to grow with a given velocity.

In section 5.2 we will show that the reduced model can be used with a time step on the order of a nanosecond. If we assume a velocity of a few mm/ns and a radius of a few mm based on Fig. 4, the length of a newly added cylindrical segment (about $v\Delta t$) is then comparable to the streamer radius.

4.4. Updating the conductivity in the channels

For simplicity, we here assume that the conductivity in the discharge channels changes according to

$$\partial_t \sigma(\mathbf{r},t) = \sigma(\mathbf{r},t)\, S(E), \tag{23}$$

where $S(E) = \bar{\alpha}\,\mu_e E$ is the electric-field dependent effective ionization rate that describes the decay (or growth) of the electron density. This approximation is justified when the conductivity is dominated by the contribution from electrons, if the electron mobility in the channel does not vary significantly, and if the main electron gain and loss processes are electron impact ionization and attachment. The change in σ due to equation (23) is computed as

$$\sigma(t+\Delta t) = e^{S\,\Delta t}\sigma(t). \tag{24}$$

Equation (23) should not be used in the high-field region near the streamer head, since the conductivity there is determined by interpolating the line conductivity given by equation (16) to the mesh using equation (3). We therefore keep track of the time at which grid cells have become part of any conductive channel, and only update those grid cells which have been inside a channel for a time τ_{delay} or more. For the examples presented in this paper, we use $\tau_{\text{delay}} = 1\,\text{ns}$.

4.5. Branching

In 3D, streamer discharges typically include multiple channels due to branching. In N_2-O_2 mixtures, the probability of branching has been shown to depend on the amount of photoionization and the applied voltage [1,37,36,38,39]. Some observations can be made based on these papers: First, branching is more likely to occur per unit length when a streamer decelerates and when its radius R decreases. Second, for thinner streamers the ratio L_{branch}/R becomes larger, where L_{branch} is the distance between consecutive branches. Below some minimum radius R, branching is unlikely.

Like [22], we here assume that branching can be described as a Poisson process, so that the time τ_{branch} until the next branching event can be sampled from the exponential distribution. We approximate the expected value of τ_{branch} as:

$$\bar{\tau}_{\text{branch}} = c_b\, \frac{R_\sigma}{v}\left(1 + \frac{L_b^2}{R_\sigma^2}\right) \tag{25}$$

where c_b and L_b are parameters. The parameter L_b controls how much $\bar{\tau}_{\mathrm{branch}}$ increases for a streamer with a small radius. For example, the branching time increases by a factor of two for $R_\sigma = L_b$, and when $R_\sigma = L_b/2$ the increase is a factor five. In case $R_\sigma \gg L_b$, c_b is approximately the ratio of the distance between branching ($L_{\mathrm{branch}} = v\,\bar{\tau}_{\mathrm{branch}}$) and the streamer radius. In the experiments of [37] the ratio L_{branch}/D was found to be about 11 ± 4, with D being the full width half maximum (FWHM) optical diameter. Based on the results presented in Appendix A we estimate that $R_\sigma \approx 0.75\,\mathrm{FWHM}$, so that $L_{\mathrm{branch}}/R_\sigma$ becomes about 15 ± 5.

Since the exponential distribution is memoryless, a new value for τ_{branch} can be sampled from the exponential distribution with rate parameter $\lambda = 1/\bar{\tau}_{\mathrm{branch}}$ every time step, and if $\tau_{\mathrm{branch}} \leq \Delta t$, branching occurs. In a branching event, an axis perpendicular to the parent branch velocity $\mathbf{v}$ is randomly sampled. An angle γ is also sampled, assumed to be uniformly distributed between 0 and 90°. The initial velocities of the two new branches are obtained by rotating $\mathbf{v}$ around the axis over angles γ and $\gamma - 90°$ respectively. However, these velocities are only used to determine the electric field directions $\hat{\mathbf{E}}(\mathbf{r}_E)$ ahead of the branches according to equations (19) and (20), and the branches propagate in the direction of $\hat{\mathbf{E}}(\mathbf{r}_E)$. The actual branching angle therefore differs from γ.

The parameters for the branching model described above were inspired by recent experimental work on streamer branching in N_2-O_2 mixtures [39]. Fig. 6 of this paper shows that in their experiments in air the typical angle between two new branches was about 90°, and this figure also suggests that the choice of angles γ and $\gamma - 90°$ is reasonable in air.

5. Results

5.1. Comparison against axisymmetric simulations

We first compare the reduced model against simulations from the dataset described in section 3.2. For the reduced model, the initial condition is zero conductivity in the whole domain. This still allows a discharge to form since equation (16) depends only on L_E, whereas in the fluid simulations some initial electrons are required. The time step used in the reduced model was set equal to the time between writing output ($\Delta t_{\mathrm{output}}$) in the fluid simulations, so that it takes about 30 steps to cross the simulation domain as discussed in section 3.1. A spatial resolution of $\Delta r = \Delta z = 0.12\,\mathrm{mm}$ was used, with a uniform mesh of 256^2 cells. Adaptive mesh refinement was not used for these cases, since the simulations already run in a few seconds on a uniform grid. As an initial condition, a streamer with a radius $R_{\sigma,0} = 0.5\,R_\sigma(L_E)$ is placed at the electrode tip, where $R_\sigma(L_E)$ is obtained according to equations (17) and (13), while L_E is determined by the electric field profile ahead of the electrode.

In Fig. 7 the conductivity profiles and electric field profiles resulting from both models are compared. The cases shown are the first eight runs of the dataset. Furthermore, Figs. 8 and 9 show the corresponding line conductivities, as defined by equation (14), and the on-axis electric field profiles. The reduced model shows good agreement regarding streamer velocity. The streamer radius agrees reasonably well too, and so do the electric field profiles. However, differences can be observed as well. For some cases, the line conductivity is almost a factor two lower near the rod electrode with the reduced model. Furthermore, the radius profile is generally more flat in the reduced model, whereas the radius in the fluid simulations initially expands. Such differences are not unexpected, since the reduced model cannot accurately describe streamer inception, and it is of course a quite simple model with only a single input L_E.

5.2. Dependence on time step and grid resolution

To study how the results of the reduced model depend on the time step, we solve the bottom case shown in Fig. 7 using time steps ranging from $\Delta t = t_{\mathrm{end}}/96 = 0.0625\,\mathrm{ns}$ up to $\Delta t = t_{\mathrm{end}}/6 = 1.0\,\mathrm{ns}$, where

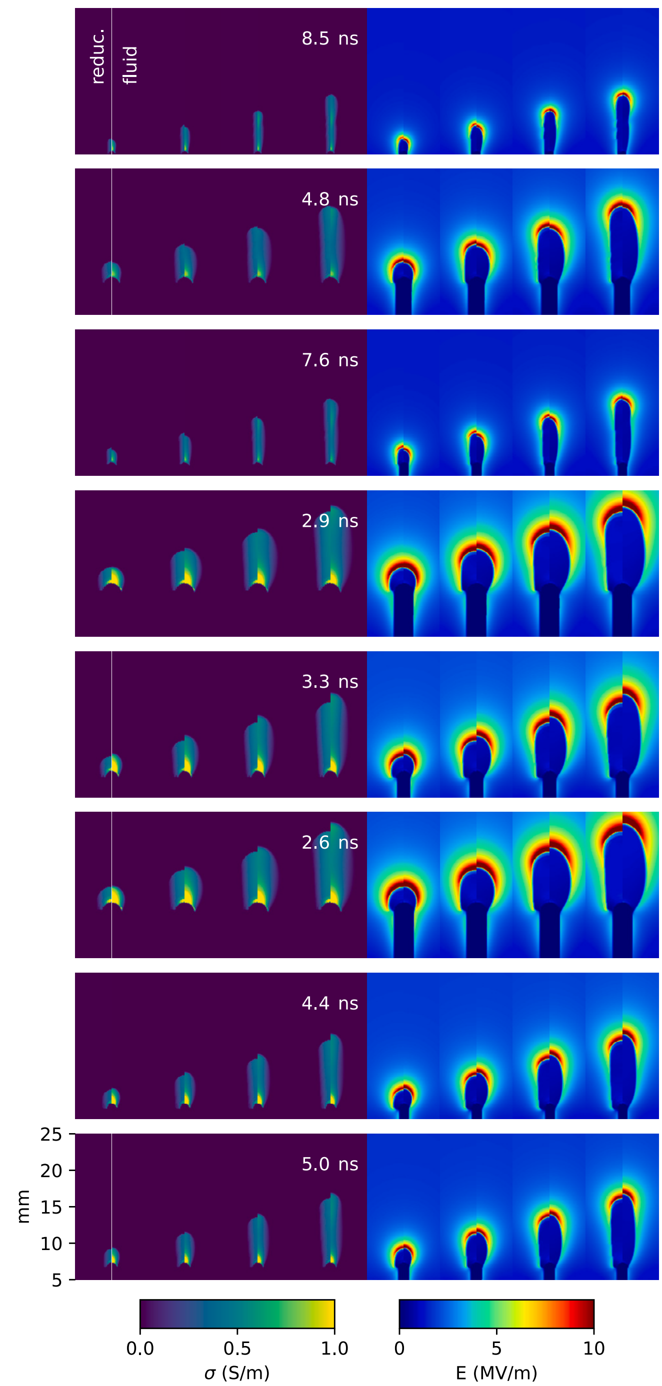

Fig. 7. Comparison of reduced model against fluid simulations, with the conductivity on the left and the electric field strength on the right. The left-halves of the sub-plots correspond to the reduced model, and the right-halves to the fluid model. Each row corresponds to one case from the simulation dataset, with output shown at 5, 10, 15 and 20 times $\Delta t_{\mathrm{output}}$, and the time at $20\,\Delta t_{\mathrm{output}}$ is shown. Note that the rod electrode, visible as the dark region in the electric field plots, varies in radius and in length for each case.

$t_{\mathrm{end}} = 6.0\,\mathrm{ns}$ (which is slightly later than the time shown in Fig. 7). The resulting line conductivity profiles and on-axis electric fields are shown in Fig. 10, using a uniform grid of 256^2 cells. For these cases, the temporal smoothing of L_E was turned off by using $\beta = 1.0$ in equation (21).

The results with the different time steps all agree rather well, showing that the reduced model is not sensitive to the time step. There is no CFL-like restriction, and the model can handle time steps much larger than the so-called dielectric relaxation time $\tau_{\mathrm{drt}} = \varepsilon_0/\sigma$ due to the im-

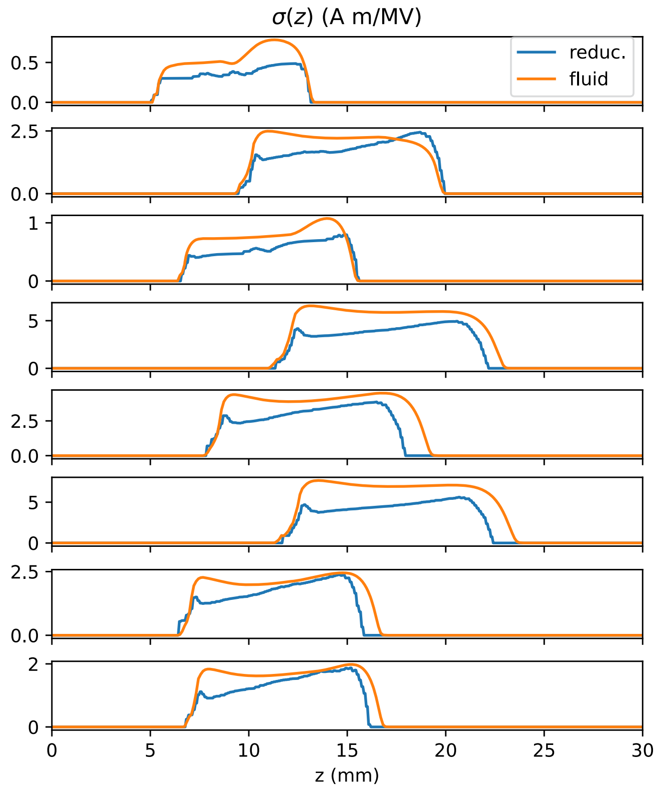

Fig. 8. Comparison of line conductivity between fluid simulations and the reduced model. The cases shown correspond to the final time states shown in Fig. 7.

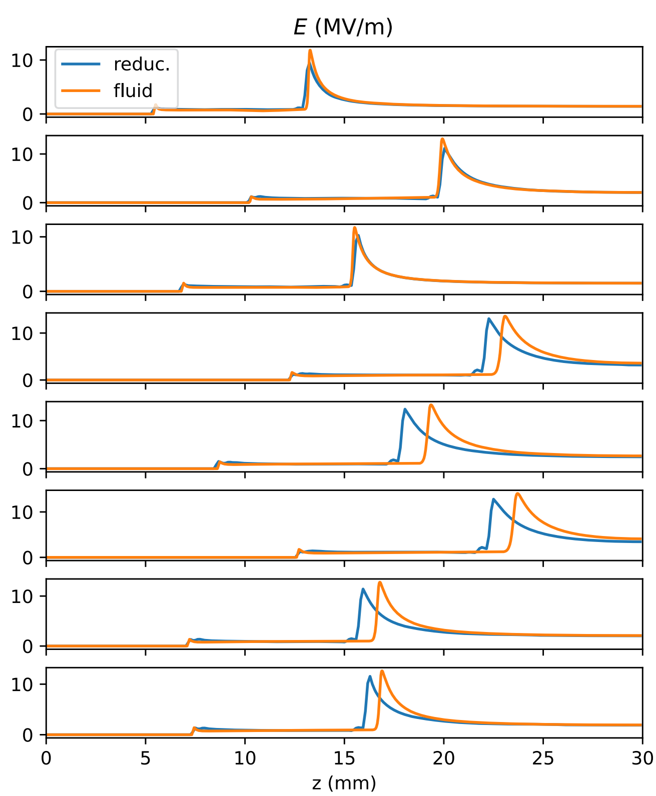

Fig. 9. Comparison of on-axis electric field between fluid simulations and the reduced model. The cases shown correspond to the final time states shown in Fig. 7.

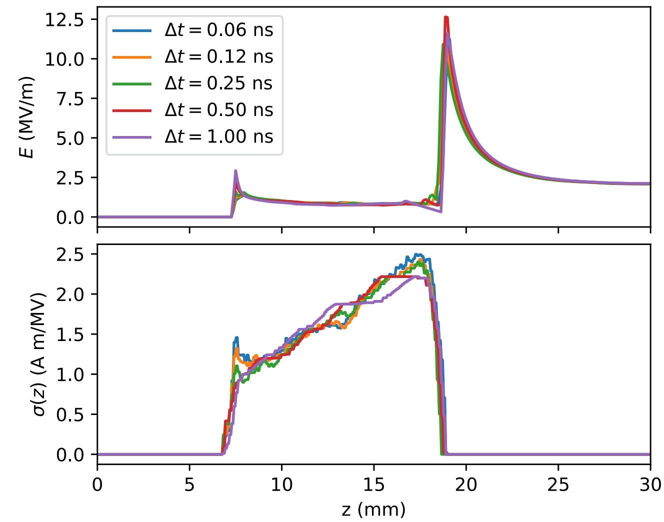

Fig. 10. The dependence of the reduced model on the time step. Shown are on-axis electric fields and the line conductivity profiles for the bottom case of Fig. 7. In the corresponding fluid simulation the time step was about 2 ps.

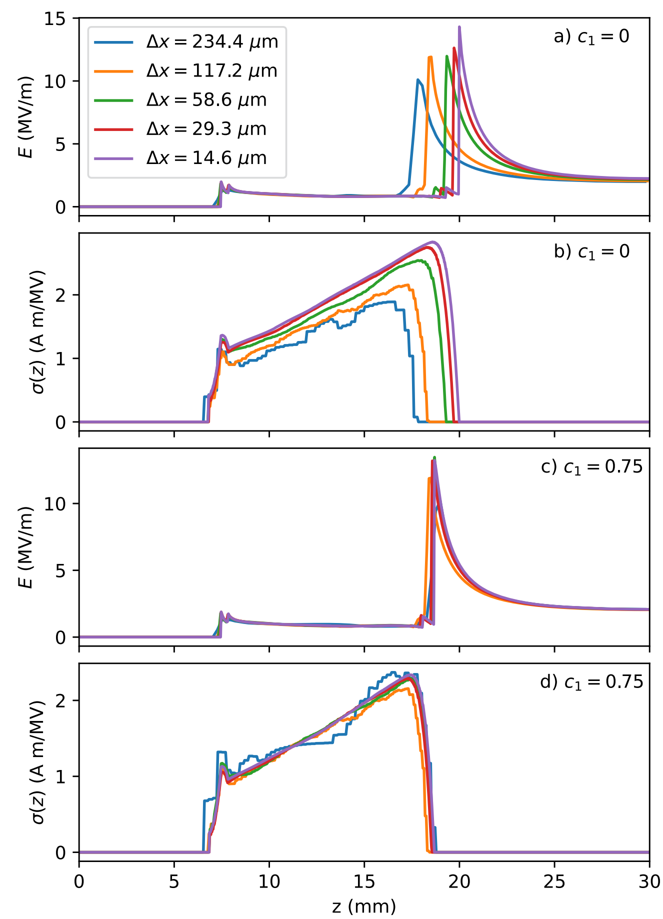

Fig. 11. The dependence of the reduced model on the grid spacing. For a) and b) no correction was included for L_E, whereas equation (26) with $c_1 = 0.75$ was used for c) and d). Shown are on-axis electric fields and the line conductivity profiles for the bottom case of Fig. 7. In the corresponding fluid simulation the finest grid spacing was 3.7 μm.

plicit solution of equation (10). In comparison, the fluid simulations had to use a time step of about 2 ps, which is almost three orders of magnitude smaller than the largest time step used in Fig. 10.

In Figs. 11a and 11b the effect of the grid resolution Δx is illustrated. The same test case was performed, with a time step of 0.25 ns, but now using a grid spacing Δx between about 15 µm (2048^2 uniform grid) and 234 µm (128^2 uniform grid). For comparison, the fluid simulations required $\Delta x = 3.7$ µm in the region around the streamer head. The variation in grid spacing has a more significant effect on the solutions than the time step. With a larger Δx the streamer velocity is lower, and there is more noise in the profiles because L_E cannot accurately be measured. The maximal electric field strength is also lower with a coarser grid since the peak value is smeared out.

The main reason for the change in velocity in Figs. 11a and 11b is that measurements of L_E depend on the grid spacing Δx. Consider for example a function that is zero for $x < x_0$ and $1 - \epsilon x$ for $x \geq x_0$, where x_0 varies and ϵ is a small positive number. If we map this function to a uniform grid with resolution Δx by averaging its value over each grid cell and then locate its maximum, the expected location will be $x_0 + \Delta x$, since if x_0 lies within a cell, the maximum will occur in the next cell. The electric field profile near the streamer head is similarly asymmetric: towards the channel it quickly drops, whereas the decay is less steep in the streamer's propagation direction. This will lead to a similar shift on the order of Δx, so that a corrected value L_E^* can be obtained as

$$L_E^* = L_E + c_1(\Delta x - \Delta x_0), \tag{26}$$

where c_1 is a constant and Δx_0 corresponds to the 256^2 grid that we used to measure L_E in the simulation dataset. Using $c_1 = 1.0$ leads to a slight over-correction, since the dependence of L_E on Δx is weaker than for the 'ideal' case mentioned above. Figs. 11c and 11d show simulation results with $c_1 = 0.75$. The streamer velocity is now much less affected by the grid spacing, and the resulting line conductivity profiles are highly similar.

5.3. 3D simulations with branching

We now perform 3D simulations in a different computational domain, measuring $(8\,\text{cm})^3$. A 4 cm long rod electrode is connected to the bottom (grounded) electrode, with a radius of 1.5 mm. The semi-spherical tip of the rod lies approximately at the center of the domain, so that discharges can grow in the 4 cm gap above it. This geometry is qualitatively similar to the 4 cm point-plane gaps used in [37,40]. In these experiments the tip of the needle was thinner, but the holder used to place the needle in probably had a larger radius than our rod.

For computational efficiency, the 3D simulations are performed with adaptive mesh refinement. A minimum grid spacing of 104 µm is used where $E \geq 30$ kV/cm. Where $E < 20$ kV/cm the mesh was derefined by a single level, so that the grid spacing is twice as large. More derefinement is possible, but then thin channels are not well resolved for visualization purposes. In contrast to conventional streamer simulations, there is no CFL condition, so the time step $\Delta t = 0.5$ ns is kept fixed regardless of the mesh spacing.

At $t = 0$, streamers with an initial radius $R_{\sigma,0} = 0.5\,R_\sigma(L_E)$ are placed at the tip of the needle electrode as discussed in section 5.1. However, we now start with multiple initial streamers, since in experiments it is also common for multiple streamers to form near a needle electrode, see e.g. [40]. The initial streamer velocities are determined in the same way as after a branching event, see section 4.5. A random angle γ and a random axis are used for each initial streamer, with the 'parent' direction assumed to be parallel to the rod's axis. In future work, the model could be extended with a stochastic criterion for streamer inception in regions with high electric field strength, instead of the manual placement of the initial streamers done here.

In Fig. 12 simulation results with an applied voltage of 40 kV and five initial streamers are shown. The branching parameters c_b and L_b are varied in this figure, with c_b between 10 and 20 and L_b between 0.2 mm and 0.8 mm. The directions of the initial streamers as well as branching processes depend on pseudorandom numbers. For each case we have performed three runs, with three different sequences of random numbers.

With larger values of c_b and L_b there is less branching. A difference is that increasing L_b reduces the branching (and thus formation) of thin channels. If L_b were zero, the number of thin branches would grow rapidly with discharge size, since the branching length L_branch would then be proportional to the channel radius, which tends to decrease as more branches form.

We can qualitatively compare our results with the experiments of [37] with a +40 kV voltage in a 4 cm gap. In the simulations the voltage is applied instantaneously, so we compare against the results with relatively fast voltage rise times of 25 to 30 ns in [37]. The velocity of the fastest simulated streamers is about 1.1 mm/ns, whereas the fastest velocities in the experiments were about 0.8 ± 0.2 mm/ns. The main reason for this discrepancy is probably the voltage rise time used in the experiments, which is comparable to the time it takes streamers to cross the gap. In [37] it was also shown that with a shorter rise time, fewer but thicker streamers form, which propagate faster. Due to the dependence of the discharge morphology on the rise time in the experiments, it is difficult to determine which values of c_b and L_b best agree with the experiments. However, there appears to be too little branching in the simulations when $L_b = 0.8$ mm or when $c_b = 20$. With $c_b = 10$ and $L_b = 0.2$ mm there is perhaps a bit too much branching, so we think that for example $c_b = 15$ and $L_b = 0.2$ mm could be reasonable.

Qualitatively, the reduced model simulations reproduce several phenomena seen in the experiments. Thin branches that are overtaken by nearby channels tend to stagnate, which limits the number of such thin branches. Furthermore, due to electrostatic repulsion, some channels that form near the electrode tip propagate almost horizontally. These channels are slower than the vertically propagating channels. Also note that the region near the electrode tip clearly has the highest conductivity. A qualitative difference is that in experiments with a fast rise time, a so-called 'inception cloud' can form around the electrode tip, see e.g. [41], which does not happen in the reduced model.

6. Discussion

6.1. Line conductivity versus line electron density

In the framework described in section 2 and in the reduced model described in section 4, we use a line conductivity σ_line. The conductivity depends on both the electron density and the electron mobility, see equation (14). The dependence of the mobility on the electric field is known, as shown in Fig. 1. From a physical point of view, it could therefore make sense to instead use the 'line electron density', obtained by integrating the electron density over a channels' cross-section. The line conductivity could then be obtained by multiplying with a field-dependent mobility. However, the main drawback of such an approach is that we have to predict the future conductivity in equation (10) without knowing the electric field, which would render this equation implicit.

6.2. Pros and cons of using a numerical mesh

An important difference between our approach and the tree model presented in [22] is that we evolve the conductivity of the discharge on a numerical mesh, whereas channels are approximated by a series of point or ring charges in the tree model, between which pair-wise electrostatic interactions are computed. An advantage of using a numerical mesh is that a standard electrostatic field solver can be used, so that existing methods for including electrodes, dielectrics and mesh refinement can be re-used. Since we resolve the streamer radius on the numerical mesh, there is also no need for the custom interaction kernels of the tree model [22,23]. A drawback of the mesh-based approach is that a relatively fine mesh is still required to simulate thin streamers. However, in terms of computational cost our model does not seem slower than the

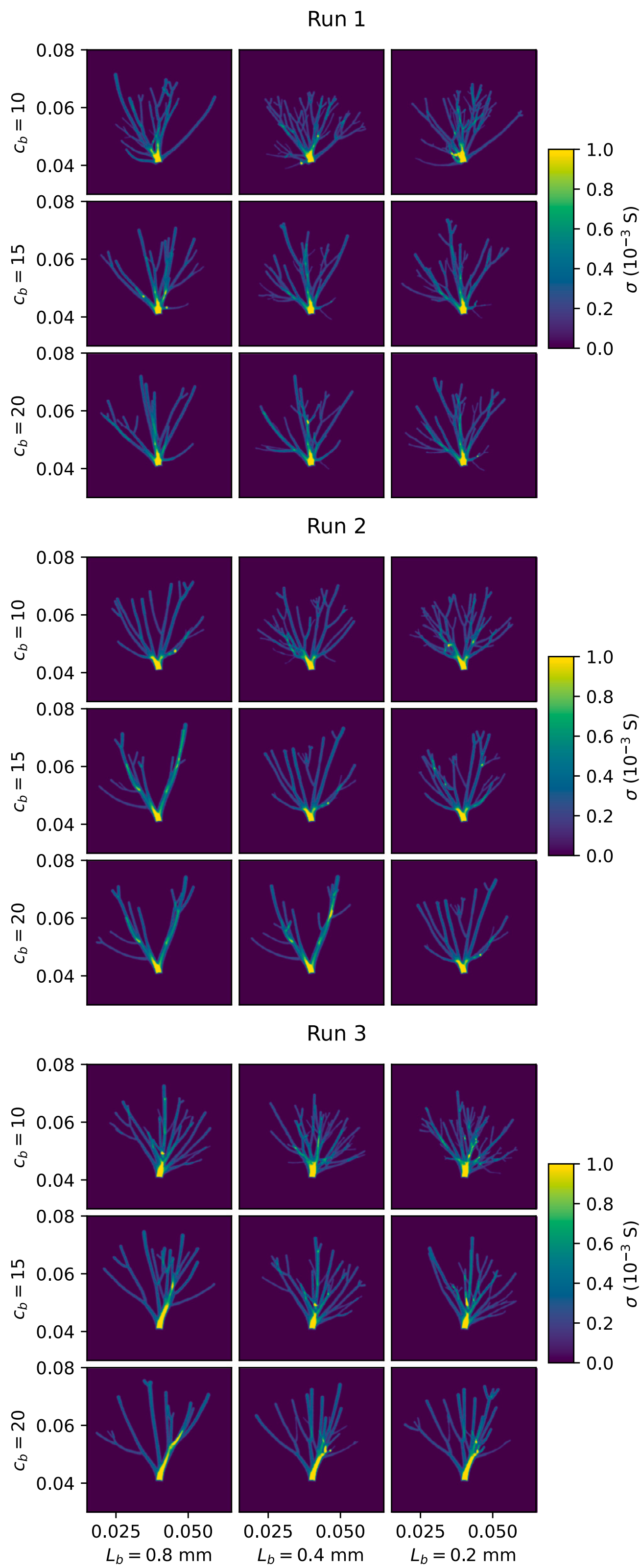

Fig. 12. 3D simulations of branching positive streamers in air with the reduced model. A needle at 40 kV was placed 4 cm below the grounded top plate. Shown is the conductivity σ at $t = 35$ ns integrated along the line-of-sight. The branching parameters c_b and L_b are varied. For each case, three runs are shown, which differ only in the sequence of pseudo-random numbers used.

tree model, since 3D simulations of similar complexity as the ones shown in section 5.3 were reported to take a few hours on a modern desktop computer with the tree model [22]. Another benefit of a mesh-based approach is that it is relatively easy to couple simulations to gas dynamics, which could be relevant to study the streamer-to-leader transition.

6.3. Computational cost of 3D simulations

The computational cost of the 3D simulations presented in section 5.3 was about 4-8 minutes per case, with the simulations running up $t = 40$ ns on a desktop computer with an AMD 2700X 8-core CPU. The majority of this CPU time was spent on solving the variable-coefficient Poisson's equation (10). Writing output to a hard disk at every time step also took quite some time, since each run produced about 10-20 GB of data. Due to the use of adaptive mesh refinement, the simulations were more expensive when there were more branches, covering a larger volume. Up to about 10^7 grid cells were used. We remark that the simulations could have been sped up by allowing for more mesh derefinement.

6.4. Conclusions and outlook

We have presented a computational framework for the simulation of filamentary electric discharges, in which the channels are represented as conducting cylindrical segments. The input for this framework is a model that predicts the position, radius and line conductivity of each channel at the next time step. This information is used to update the electric conductivity on a numerical mesh, from which the electric potential at the next time step is computed by solving a variable-coefficient Poisson equation. An existing field solver [24] is used for this purpose, which supports adaptive mesh refinement and parallelization. To allow for easy experimentation with different types of models, the computationally expensive components of the framework are written in Fortran but compiled into a Python module.

To demonstrate how the framework can be used, we have generated a dataset of 1000 axisymmetric positive streamer simulations in air at 1 bar, by varying the applied voltage and the electrode geometry. The simulations were performed with a drift-diffusion fluid model and the local field approximation, using applied voltages between 36 kV and 60 kV in a 30 mm gap. The needle electrode length was varied between 4.5 mm and 12 mm. Based on the simulation data, simple fit expressions were presented for the streamer radius, velocity and line conductivity. These fits depend on a single input feature, which measured the size of the high-field region ahead of the streamer.

Based on the computational framework and the fitted expressions, a reduced model for positive streamers in air was presented. In this model, streamers are assumed to propagate parallel to the electric field, and branching is included a stochastic process described by two parameters. The reduced model was compared against axisymmetric simulations from the dataset, and it generally showed good agreement despite its simplicity. We demonstrated that the spatial and temporal step sizes can be several orders of magnitude larger in the reduced model than in the classical fluid model, and that the reduced model is not sensitive to these step sizes.

Finally, we have presented 3D simulations with the reduced model, using a 4 cm needle-plate gap with an applied voltage of 40 kV, similar to the geometry used in some of the experiments presented in [37]. In the simulations the streamer velocity was about 30% higher than in the experiments, which we mainly attributed to the voltage rise time in the experiments. The effect of the branching parameters was studied, and similar discharge morphologies were observed as in the experiments. However, it should be mentioned that the experimental results were quite sensitive to the voltage rise time, so we could not accurately determine values for the branching parameters. The cost of the 3D simulations was rather modest, with individual runs taking 4-8 minutes on a desktop computer, depending on the complexity of the discharge.

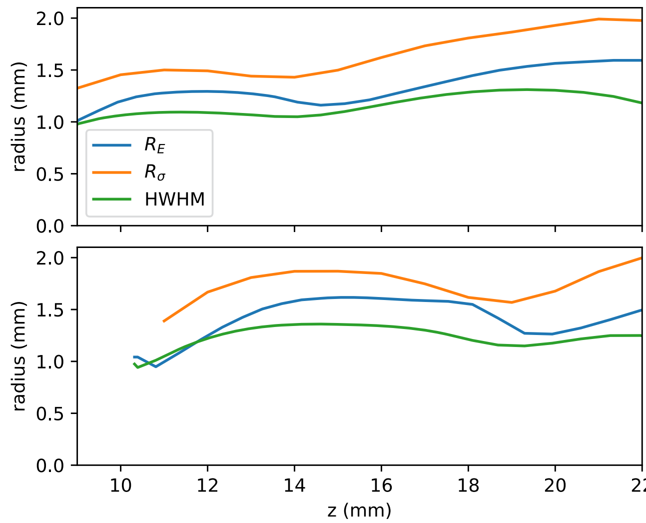

Fig. A.13. Comparison of different definitions of the streamer radius (see text) versus the z-coordinate of the streamer head, for two of the cases from the dataset described in section 3.2.

The parameters of the model presented here could be improved by comparing against experiments, in particular regarding streamer branching. Perhaps similar models can also be developed for gases other than air, in which branching is typically more frequent. In future work, it would also be interesting to experiment with different discharge models, for example a physics-based reduced model [42] or a more sophisticated machine-learning model. Negative streamers could also be considered in the future. Another option would be to study the streamer-to-leader transition with the reduced model, which could then be coupled to equations for gas dynamics.

CRediT authorship contribution statement

Jannis Teunissen: Writing – original draft, Software, Methodology, Investigation, Formal analysis, Data curation, Conceptualization. **Alejandro Malagón-Romero:** Writing – review & editing, Software, Methodology, Investigation, Funding acquisition, Formal analysis, Conceptualization.

Declaration of competing interest

The authors declare the following financial interests/personal relationships which may be considered as potential competing interests: Alejandro Malagon-Romero reports financial support was provided by Ramón Areces Foundation. If there are other authors, they declare that they have no known competing financial interests or personal relationships that could have appeared to influence the work reported in this paper.

Acknowledgements

A.M.R. was supported by a Ramón Areces Foundation grant No. BEVP34A6840. The reduced discharge model described in this paper is available at https://github.com/jannisteunissen/cocydimo and the simulation dataset is available at https://doi.org/10.5281/zenodo.15296406.

Appendix A. Comparison of different streamer radius definitions

There are quite a few different definitions of the streamer radius, see e.g. [43,44]. We here consider three definitions of the radius:

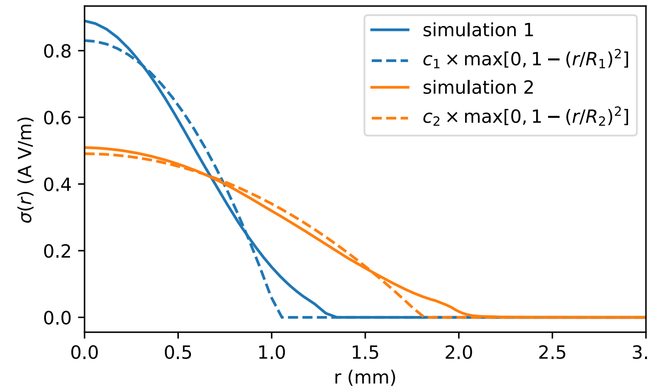

Fig. A.14. Two examples of radial conductivity profiles from simulations together with fitted curves assuming a radial profile as given by equation (5).

- The electrodynamic radius R_E, defined as the radial coordinate at which the radial electric field E_r has a maximum.
- The radius R_σ of the streamer's radial conductivity profile, found by fitting the radial conductivity profile with a function of the form

$$f(r) = c\ \max\left(0, 1-(r/R_\sigma)^2\right), \tag{A.1}$$

  similar to equation (5).
- The optical radius, defined as the "Half Width at Half Maximum" (HWHM) of the time-integrated optical emission, after applying a Forward Abel transform on the axisymmetric simulation data.

Fig. A.13 shows a comparison of these definitions for two of the simulations in our dataset. It can be seen that R_σ is typically about 10% to 30% larger than R_E, and that R_σ is typically about 30% to 40% larger than HWHM. Based on these observations, we use the rather rough approximation $R_\sigma = 1.2\,R_E$ in this paper. Finally, Fig. A.14 shows two examples of radial conductivity profiles from our simulation dataset together with fitted curves according to equation (A.1).

Data availability

The reduced discharge model described in this paper is available at https://github.com/jannisteunissen/cocydimo and the simulation dataset is available at https://doi.org/10.5281/zenodo.15296406.

References

[1] Sander Nijdam, Jannis Teunissen, Ute Ebert, The physics of streamer discharge phenomena, Plasma Sources Sci. Technol. 29 (10) (November 2020) 103001.
[2] A. Bourdon, Z. Bonaventura, S. Celestin, Influence of the pre-ionization background and simulation of the optical emission of a streamer discharge in preheated air at atmospheric pressure between two point electrodes, Plasma Sources Sci. Technol. 19 (3) (May 2010) 034012.
[3] M.M. Becker, D. Loffhagen, Enhanced reliability of drift-diffusion approximation for electrons in fluid models for nonthermal plasmas, AIP Adv. 3 (1) (January 2013) 012108.
[4] A. Luque, U. Ebert, Density models for streamer discharges: beyond cylindrical symmetry and homogeneous media, J. Comput. Phys. 231 (3) (February 2012) 904–918.
[5] Atsushi Komuro, Shuto Matsuyuki, Akira Ando, Simulation of pulsed positive streamer discharges in air at high temperatures, Plasma Sources Sci. Technol. 27 (10) (October 2018) 105001.
[6] Robert Marskar, An adaptive Cartesian embedded boundary approach for fluid simulations of two- and three-dimensional low temperature plasma filaments in complex geometries, J. Comput. Phys. 388 (July 2019) 624–654.
[7] Robert Marskar, 3D fluid modeling of positive streamer discharges in air with stochastic photoionization, Plasma Sources Sci. Technol. 29 (5) (May 2020) 055007.
[8] Ryo Ono, Atsushi Komuro, Generation of the single-filament pulsed positive streamer discharge in atmospheric-pressure air and its comparison with two-dimensional simulation, J. Phys. D, Appl. Phys. 53 (3) (January 2020) 035202.
[9] Zhen Wang, Anbang Sun, Sasa Dujko, Ute Ebert, Jannis Teunissen, 3D simulations of positive streamers in air in a strong external magnetic field, Plasma Sources Sci. Technol. (January 2024).

[10] M. Jiang, Y. Li, H. Wang, C. Liu, 3D PIC-MCC simulations of positive streamers in air gaps, Phys. Plasmas 24 (10) (October 2017) 102112.

[11] B. Bagheri, J. Teunissen, U. Ebert, M.M. Becker, S. Chen, O. Ducasse, O. Eichwald, D. Loffhagen, A. Luque, D. Mihailova, J.M. Plewa, J. van Dijk, M. Yousfi, Comparison of six simulation codes for positive streamers in air, Plasma Sources Sci. Technol. 27 (9) (September 2018) 095002.

[12] Phelps database, www.lxcat.net, retrieved on August 19, 2021.

[13] L.C. Pitchford, A.V. Phelps, Comparative calculations of electron-swarm properties in N 2 at moderate E N values, Phys. Rev. A 25 (1) (January 1982) 540–554.

[14] C. Montijn, W. Hundsdorfer, U. Ebert, An adaptive grid refinement strategy for the simulation of negative streamers, J. Comput. Phys. 219 (2) (December 2006) 801–835.

[15] S. Pancheshnyi, P. Ségur, J. Capeillère, A. Bourdon, Numerical simulation of filamentary discharges with parallel adaptive mesh refinement, J. Comput. Phys. 227 (13) (June 2008) 6574–6590.

[16] V.I. Kolobov, R.R. Arslanbekov, Towards adaptive kinetic-fluid simulations of weakly ionized plasmas, J. Comput. Phys. 231 (3) (February 2012) 839–869.

[17] Jannis Teunissen, Ute Ebert, Simulating streamer discharges in 3D with the parallel adaptive Afivo framework, J. Phys. D, Appl. Phys. 50 (47) (October 2017) 474001.

[18] L. Niemeyer, L. Pietronero, H. Wiesmann, Fractal dimension of dielectric breakdown, Phys. Rev. Lett. 52 (12) (March 1984) 1033–1036.

[19] Victor P. Pasko, Umran S. Inan, Timothy F. Bell, Fractal structure of sprites, Geophys. Res. Lett. 27 (4) (February 2000) 497–500.

[20] M.D. Noskov, M. Sack, A.S. Malinovski, A.J. Schwab, Measurement and simulation of electrical tree growth and partial discharge activity in epoxy resin, J. Phys. D, Appl. Phys. 34 (9) (May 2001) 1389–1398.

[21] Mose Akyuz, Anders Larsson, Vernon Cooray, Gustav Strandberg, 3D simulations of streamer branching in air, J. Electrost. 59 (2) (September 2003) 115–141.

[22] Alejandro Luque, Ute Ebert, Growing discharge trees with self-consistent charge transport: the collective dynamics of streamers, New J. Phys. 16 (1) (January 2014) 013039.

[23] A. Luque, M. González, F.J. Gordillo-Vázquez, Streamer discharges as advancing imperfect conductors: inhomogeneities in long ionized channels, Plasma Sources Sci. Technol. 26 (12) (November 2017) 125006.

[24] Jannis Teunissen, Ute Ebert, Afivo: a framework for quadtree/octree AMR with shared-memory parallelization and geometric multigrid methods, Comput. Phys. Commun. 233 (December 2018) 156–166.

[25] A. Luque, H.C. Stenbaek-Nielsen, M.G. McHarg, R.K. Haaland, Sprite beads and glows arising from the attachment instability in streamer channels: DYNAMICS OF SPRITE CHANNELS, J. Geophys. Res. Space Phys. 121 (3) (March 2016) 2431–2449.

[26] Peter L.G. Ventzek, Two-dimensional modeling of high plasma density inductively coupled sources for materials processing, J. Vac. Sci. Technol. B 12 (1) (January 1994) 461.

[27] G.J.M. Hagelaar, G.M.W. Kroesen, Speeding up fluid models for gas discharges by implicit treatment of the electron energy source term, J. Comput. Phys. 159 (1) (March 2000) 1–12.

[28] Jannis Teunissen, Francesca Schiavello, Geometric multigrid method for solving Poisson's equation on octree grids with irregular boundaries, Comput. Phys. Commun. 286 (May 2023) 108665.

[29] Hank Childs, Eric Brugger, Brad Whitlock, Jeremy Meredith, Sean Ahern, David Pugmire, Kathleen Biagas, Mark Miller, Cyrus Harrison, Gunther H. Weber, Hari Krishnan, Thomas Fogal, Allen Sanderson, Christoph Garth, E. Wes Bethel, David Camp, Oliver Rübel, Marc Durant, Jean M. Favre, Paul Navrátil, VisIt: an end-user tool for visualizing and analyzing very large data, in: High Performance Visualization–Enabling Extreme-Scale Scientific Insight, Chapman and Hall/CRC, October 2012, pp. 357–372.

[30] Xiaoran Li, Siebe Dijcks, Sander Nijdam, Anbang Sun, Ute Ebert, Jannis Teunissen, Comparing simulations and experiments of positive streamers in air: steps toward model validation, Plasma Sources Sci. Technol. 30 (9) (September 2021) 095002.

[31] G.J.M. Hagelaar, L.C. Pitchford, Solving the Boltzmann equation to obtain electron transport coefficients and rate coefficients for fluid models, Plasma Sources Sci. Technol. 14 (4) (November 2005) 722–733.

[32] M.B. Zheleznyak, A.K. Mnatsakanian, S.V. Sizykh, Photoionization of nitrogen and oxygen mixtures by radiation from a gas discharge, Teplofiz. Vys. Temp. 20 (November 1982) 423–428.

[33] S.V. Pancheshnyi, A. Yu Starikovskii, Stagnation dynamics of a cathode-directed streamer discharge in air, Plasma Sources Sci. Technol. 13 (3) (August 2004) B1–B5.

[34] M. Niknezhad, O. Chanrion, J. Holbøll, T. Neubert, Underlying mechanism of the stagnation of positive streamers, Plasma Sources Sci. Technol. 30 (11) (November 2021) 115014.

[35] Xiaoran Li, Baohong Guo, Anbang Sun, Ute Ebert, Jannis Teunissen, A computational study of steady and stagnating positive streamers in N2–O2 mixtures, Plasma Sources Sci. Technol. (2022) 15.

[36] S. Nijdam, F.M.J.H. van de Wetering, R. Blanc, E.M. van Veldhuizen, U. Ebert, Probing photo-ionization: experiments on positive streamers in pure gases and mixtures, J. Phys. D, Appl. Phys. 43 (14) (April 2010) 145204.

[37] T.M.P. Briels, J. Kos, G.J.J. Winands, E.M. van Veldhuizen, U. Ebert, Positive and negative streamers in ambient air: measuring diameter, velocity and dissipated energy, J. Phys. D, Appl. Phys. 41 (23) (November 2008) 234004.

[38] Zhen Wang, Siebe Dijcks, Yihao Guo, Martijn Van Der Leegte, Anbang Sun, Ute Ebert, Sander Nijdam, Jannis Teunissen, Quantitative modeling of streamer discharge branching in air, Plasma Sources Sci. Technol. 32 (8) (August 2023) 085007.

[39] Yihao Guo, Sander Nijdam, Statistical analysis on branching characteristics of positive streamer discharges in N_2 –O_2 mixtures, Plasma Sources Sci. Technol. 33 (4) (April 2024) 045006.

[40] T.M.P. Briels, E.M. van Veldhuizen, U. Ebert, Positive streamers in air and nitrogen of varying density: experiments on similarity laws, J. Phys. D, Appl. Phys. 41 (23) (December 2008) 234008.

[41] She Chen, L.C.J. Heijmans, Rong Zeng, S. Nijdam, U. Ebert, Nanosecond repetitively pulsed discharges in N_2 –O_2 mixtures: inception cloud and streamer emergence, J. Phys. D, Appl. Phys. 48 (17) (May 2015) 175201.

[42] Dennis Bouwman, Jannis Teunissen, Ute Ebert, Macroscopic parameterization of positive streamer heads in air, Plasma Sources Sci. Technol. 34 (2025) 025015.

[43] S. Pancheshnyi, M. Nudnova, A. Starikovskii, Development of a cathode-directed streamer discharge in air at different pressures: experiment and comparison with direct numerical simulation, Phys. Rev. E (3) 71 (1) (January 2005).

[44] Baohong Guo, Xiaoran Li, Ute Ebert, Jannis Teunissen, A computational study of accelerating, steady and fading negative streamers in ambient air, Plasma Sources Sci. Technol. 31 (9) (September 2022) 095011.